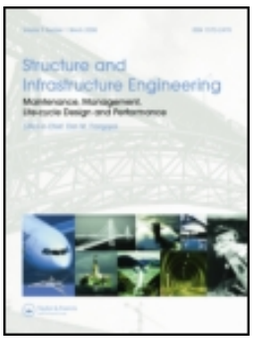

Taylor & Francis
Taylor & Francis Group

Structure and Infrastructure Engineering
Maintenance, Management, Life-Cycle Design and Performance

ISSN: 1573-2479 (Print) 1744-8980 (Online) Journal homepage: https://www.tandfonline.com/loi/nsie20

Behaviour of the reinforced concrete face slabs of concrete faced rockfill dams during impounding

Yalin Arici

To cite this article: Yalin Arici (2013) Behaviour of the reinforced concrete face slabs of concrete faced rockfill dams during impounding, Structure and Infrastructure Engineering, 9:9, 877-890, DOI: 10.1080/15732479.2011.631111

To link to this article: https://doi.org/10.1080/15732479.2011.631111

Published online: 17 Nov 2011.

Submit your article to this journal

Article views: 221

View related articles

Citing articles: 5 View citing articles

Full Terms & Conditions of access and use can be found at
https://www.tandfonline.com/action/journalInformation?journalCode=nsie20

Structure and Infrastructure Engineering
Vol. 9, No. 9, September 2013, 877–890

Taylor & Francis
Taylor & Francis Group

Behaviour of the reinforced concrete face slabs of concrete faced rockfill dams during impounding

Yalin Arici*

Structural Mechanics Laboratory K2-303, Department of Civil Engineering, Middle East Technical University, Ankara 06800, Turkey

(*Received 2 May 2011; final version received 1 September 2011; accepted 29 September 2011; published online 17 November 2011*)

The primary goal of this study was to examine the relative effects of various factors that affect the cracking of the face slab of a concrete faced rockfill dam (CFRD). Rigorous simulation of the construction and impoundment stages were conducted in sequential phases during which the rockfill and the rockfill-face slab interface were modelled with elasto-plastic models that were calibrated to existing test data. The face slab was modelled using embedded reinforcements with a total strain crack model. The results of the analyses showed that the stiffness of the rockfill significantly changed the crackwidth on the face slab, but not the extent of cracking. Increasing the reinforcement ratio was the most effective remedy for decreasing the average crack width on the slab. The properties of the rockfill-slab interface and the location of the reinforcement within the slab did not significantly affect the cracking on the slab.

Keywords: concrete faced rockfill dams; design; cracking; clear cover; face slab; reinforcement ratio

List of Symbols

A	Equivalent area encasing a single bar
d_c	Clear cover thickness
E	Young's modulus
f_c	Concrete peak compressive strength
f_t	Concrete peak tensile strength
f_y	Steel yield stress
G_f^I	Concrete fracture energy
G_{ref}	Reference shear modulus
h	Concrete effective element size
K_{ref}	Reference compression modulus
m	Material parameter for non-linear elasticity
p'	Effective mean stress
$\mathbf{R}$	6×6 factor matrix used in rockfill plasticity formulation
p_a	Atmospheric pressure
p'_t	Compression offset used in non-linear elasticity for rockfill constitutive model
p_c	Preconsolidation pressure
q'	Effective deviatoric stress
t_n, t_t	Normal and tangential tractions for the interface elements
$w_{\max}$	Crack width
β_1	Internal parameter for rockfill elasto-plastic model
β_{GL}	Strain gradient factor for Gergely–Lutz formula
$\Delta p'$	Pressure shift for the shear yield surface in rockfill elasto-plastic model
$\Delta\gamma^p$	Equivalent plastic strain increment
ε	Strain tensor
ε_v^e	Elastic volumetric strain
ε_v	Plastic volumetric strain
ε_v	Volumetric strain
ε_y	Steel yield strain
ε_{scr}	Reinforcement strain
ϕ	Friction angle
ϕ_I	Friction angle of the interface
ϕ_{cv}	Friction angle at constant volume for rockfill elasto-plastic model
γ	Deviatoric strain vector
κ_1	Internal model variable for tracking of hardening behaviour of shear failure surface
$\dot{\lambda}$	Interface element internal model parameter
θ	Lode's angle
ϑ	Dilation angle for rockfill
ϑ_1	Dilation angle for the interface
υ	Poisson ratio

1. Introduction

Concrete faced rockfill dam (CFRD) is a popular choice in some countries because of certain advantages over the clay-core earthfill and concrete dams. The

*Email: yarici@metu.edu.tr

ISSN 1573-2479 print/ISSN 1744-8980 online
© 2013 Taylor & Francis
http://dx.doi.org/10.1080/15732479.2011.631111
http://www.tandfonline.com

structural and geotechnical design of CFRDs are based on precedence (Cooke 1986) with little emphasis on using analytical tools to predict the performance of the face slab. By ensuring the stability of the embankment using conventional slope stability analyses, the thickness of the face slab, as well as the reinforcement ratio, is usually chosen based on empirical formulas (ICOLD 2004, Qian 2005). Recent experiences in two major dam projects, i.e. the ZipingPu Dam in China (Wieland 2010) after an earthquake excitation and the Mohale Dam in Lesotho (Johannesson and Tohlang 2007) immediately after impounding, emphasised the importance of conducting more field and laboratory research of CFRDs, especially to develop analytical approaches in predicting the complex behaviour of these systems using advanced constitutive models.

Understanding the behaviour of a CFRD is a challenging task as the behaviour is shaped by the complex interaction between various components of the dam, namely the rockfill, the cushion layer-face slab interface and the concrete face slab. The rockfill, as summarised in the literature review by Varadarajan *et al*. (2003), exhibits a highly non-linear response with its mechanical properties strongly dependent on the confining pressure. The transfer of the shear force between the slab and the cushion layer is a friction/contact problem as described in the studies by Zhang and Zhang (2009) and Uesugi *et al*. (1990). The complex interaction of these components were perhaps first simulated by Uddin (1999) with some simplifications (assuming the interface and the face slab behaviours are linear-elastic and the fill behaviour is elasto-plastic) using a plane strain model. The tensile stresses obtained in this study (as high as 20 MPa) were beyond the acceptable levels showing significant cracking of the concrete face slab may be an issue for a CFRD. Considering the reservoir interaction for the rockfill, principal tensile stresses on the order of 5 MPa were obtained for the face slab in Bayraktar and Kartal (2010). Zhang and Zhang (2009) employed a hardening elasto-plastic model with two yield surfaces for the rockfill, a softening model for the interface and linear elastic concrete elements for the simulation of a CFRD. Their results showed that the compressive stresses on the face slab were altered to tensile stresses as high as 4 MPa during an earthquake event. The high tensile stresses obtained on the slab in these studies shows that the face slab is likely to crack; however, the cracking phenomena and its relation to the performance of the CFRD have not been investigated sufficiently in the past.

The primary goal of this article is to investigate the performance of the face slab of a CFRD during impounding considering the variability in the factors affecting its performance. The factors that affect the performance of a CFRD are considered in two parts: (1) Embankment-related factors, i.e. the stiffness of the rockfill and the properties of the rockfill-face slab interface and (2) the design choices for the face slab including the reinforcement ratio, thickness of the face slab, concrete strength and the clear cover thickness (location of reinforcement within the slab). Considering the possible variability in the factors provided above, the cracking of the slab was investigated using a 2D plane-strain model. The construction sequence for the dam as well as the incremental rise of the reservoir was properly represented in the simulations. The rockfill was modelled using a two-surface elasto-plastic model incorporating non-linear elasticity whereas the face slab was modelled using a total strain crack model with embedded reinforcements. The interface between the face slab and the rockfill was modelled using a friction/contact model capable of simulating the sliding/dilating behaviour. Using these advanced constitutive models, the extent of the cracked region and the maximum crack width within the crack region were investigated with the purpose of determining (1) the factors leading to excessive cracking of the face slab and (2) the design recommendations to successfully address this problem.

There are some limitations to this study. First of all, the deformations of the face plate parallel to the dam axis or the opening of the vertical construction joints cannot be predicted within the scope of this work. The effect of the loading on the slabs near the valley boundaries (at the abutments) cannot be investigated with this model as well. Investigation of these issues would require a detailed 3D model of the system which is intended for future work.

2. Case study: Cokal dam

The CFRD under investigation herein is the Cokal dam, an 83-m high CFRD with a crest length of 605 m, located in north–west Turkey in the Thracian peninsula. Positioned in a wide canyon, the dam geometry permits the use of the plane-strain analogy utilised in this study. A typical cross-section of the dam is shown in Figure 1a along with a selection of the materials that will be used at the site. The face slab of the Cokal dam is planned to be 50 cm thick with a 0.3% reinforcement ratio, based on the face slab designs used in similar dams.

The Cokal dam was modelled and analysed using the general purpose finite element software DIANA (TNO DIANA 2008). A total of 4600 six-node isoparametric plane-strain triangular elements with a three-point integration scheme were used in modelling the rockfill, whereas 54 three-node infinite shell elements, with each node having two translational

and one rotational degree of freedom, were used to represent the face slab. The infinite shell formulation, based on the isoparametric degenerated solid approach given in TNO DIANA (2008), introduces two shell hypotheses, i.e. the normals remain straight in the element and the stress perpendicular to the axis of the element is zero. Embedded reinforcements, which do not have degrees of freedom of their own, are smeared in the face slab elements. The strains of the embedded reinforcement elements are computed from the displacement field of the mother element, implying a perfect bond between the reinforcement and the material. The face slab elements were connected to the rockfill with the line interface elements, based on

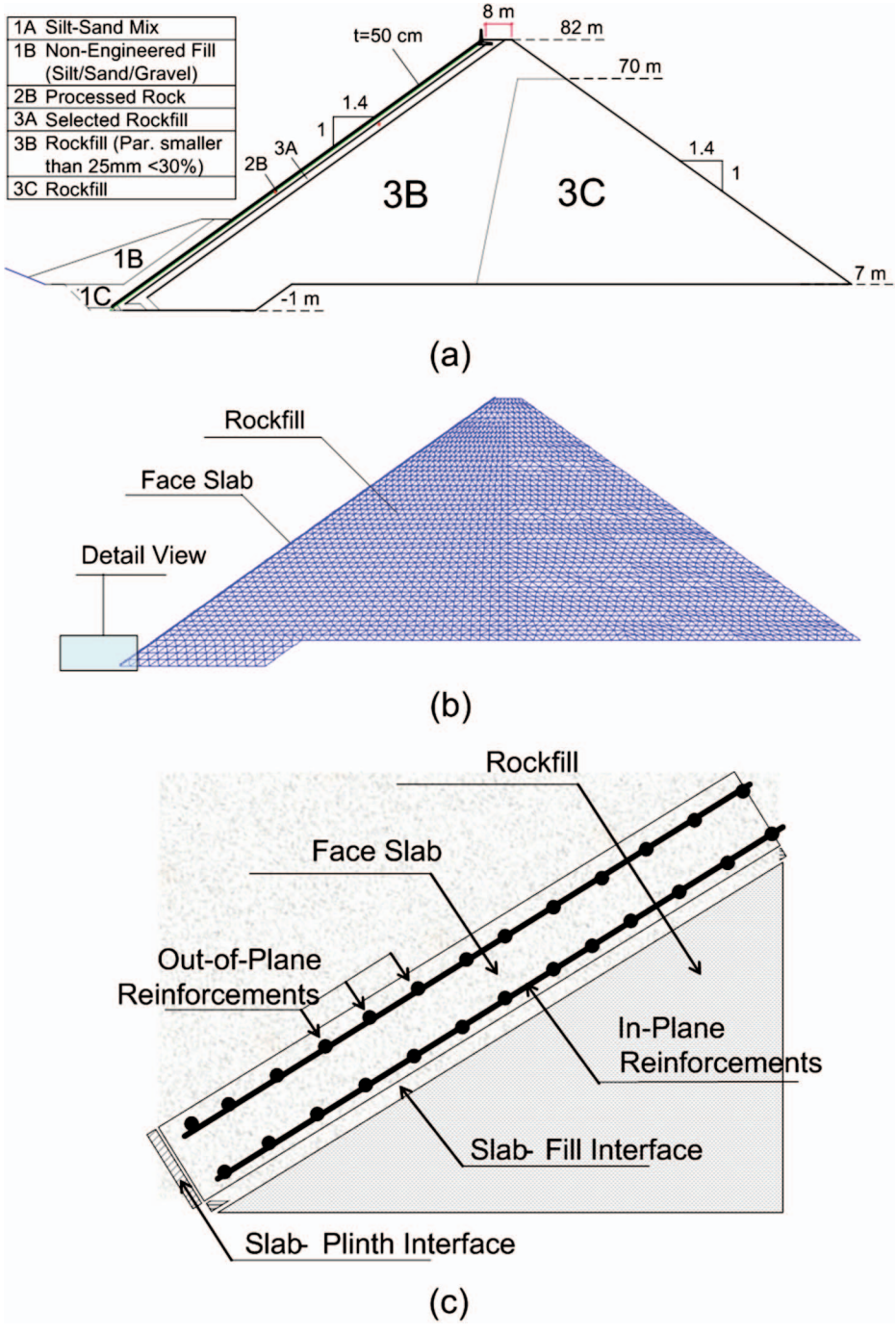

Figure 1. The Cokal dam and the finite element model. (a) Cokal dam preliminary design; (b) Cokal dam finite element model; (c) finite element model detail.

quadratic interpolation, describing the relationship between the normal and shear stresses and the relative normal and shear displacements at multiple nodes. A nodal interface element was used at the bottom of the face slab to properly model any possible separation from the foundation at the plinth. The Cokal dam rests on medium-hard rock with a Young's modulus that is approximately two orders of magnitude greater than that of the dam material; therefore, the foundation of the dam was not included in the model, and the base was assumed to be a fixed support. A sketch of the modelled constituents of the Cokal dam is shown in Figure 1c.

3. Constitutive relationships

3.1. Reinforced concrete

The constitutive model used for concrete is based on the total strain fixed-crack model (Feenstra *et al.* 1998). The basic concept of the total strain crack models is that the stress is evaluated in the directions that are given by the crack directions. For the fixed crack model, the stress–strain relationships are evaluated in a coordinate system that is fixed upon cracking. The strain vector $\boldsymbol{\varepsilon}_{\mathbf{xyz}}(t_i)$ is updated with the strain increment $\boldsymbol{\Delta\varepsilon}_{\mathbf{xyz}}(t_i + \Delta t_i)$ in the element coordinate system as follows:

$$\boldsymbol{\varepsilon}_{\mathbf{xyz}}(t_i + \Delta t_i) = \boldsymbol{\varepsilon}_{\mathbf{xyz}}(t_i) + \Delta\boldsymbol{\varepsilon}_{\mathbf{xyz}}(t_i + \Delta t_i). \quad (1)$$

The strain $\boldsymbol{\varepsilon}_{\mathbf{xyz}}(t_i + \Delta t_i)$ is transformed to the strain vector in the crack directions $\boldsymbol{\varepsilon}_{\mathrm{nst}}(t_i + \Delta t_i) = \mathbf{T}\boldsymbol{\varepsilon}_{\mathbf{xyz}}(t_i + \Delta t_i)$ with the transformation matrix $\mathbf{T}$. The constitutive model is then used within the crack coordinate system which is given by:

$$\boldsymbol{\sigma}_{\mathbf{nst}}(t_i + \Delta t_i) = \boldsymbol{\sigma}(\boldsymbol{\varepsilon}_{\mathbf{nst}}(t_i + \Delta t_i)). \quad (2)$$

The updated stress vector in the element coordinate system is given by the transformation:

$$\boldsymbol{\sigma}_{\mathbf{xyz}}(t_i + \Delta t_i) = \mathbf{T}^T\boldsymbol{\sigma}_{\mathbf{nst}}(\boldsymbol{\varepsilon}_{\mathbf{nst}}(t_i + \Delta t_i)). \quad (3)$$

The compressive behaviour was defined by a parabolic response, with f_c defining the peak strength (Figure 2). The crushing behaviour and the ultimate strain are governed by the compressive fracture energy G_c so that the model is objective and mesh-independent. The tensile behaviour was modelled by using a linear softening function beyond the tensile strength f_t, with the ultimate tensile strain based on the tensile fracture energy G_f^I. The utilised tensile-compressive constitutive relationships are presented in Figure 2a and b, respectively, with h denoting the effective element size. A typical strain hardening diagram was chosen for the embedded reinforcement with the stress–strain diagram as given in Figure 2c, where f_y and ε_y represent the yield strength and strain, respectively.

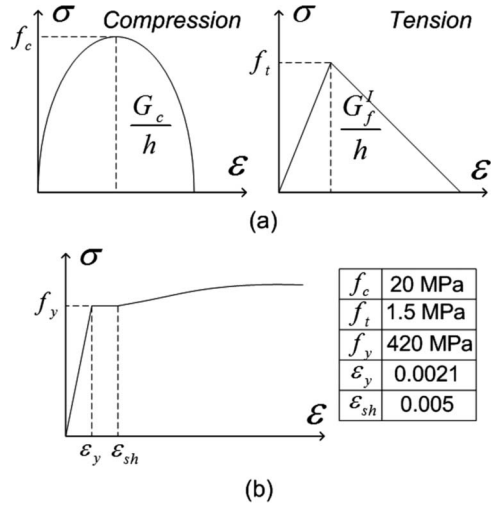

Figure 2. Constitutive relationships for the reinforced concrete face slab. (a) Concrete stress–strain relationship; (b) steel stress–strain relationship.

3.2. Rockfill

Triaxial tests conducted on rockfill specimens reveal the following (Varadarajan *et al.* 2003): (1) the stress–strain behaviour of rockfill material is nonlinear, inelastic and stress-dependent; (2) an increase in the confining pressure tends to increase the values of the peak deviatoric stress, axial strain and volumetric strain at failure and (3) an increase in the size of the particles results in an increase in the volumetric strain at the same confining pressure. The strength envelope of rockfill specimens is curved: an increase in the confining stress leads to a diminishing increase in the deviatoric stress for higher confining stress levels, signifying the decrease of the friction angle with the confining pressure. A modified Mohr-Coulomb formulation (Groen 1994), as implemented in TNO DIANA (2008), was used in this study to model (1) the hardening of the rockfill with increasing shear stress, (2) the volumetric deformations and (3) the dependency of the mechanical properties on the confinement stress. This constitutive relationship utilises non-linear elasticity combined with a smooth, hardening shear yield surface and a circular-shaped compression cap.

Elastic behaviour is assumed to be isotropic in this model. The tangent compression modulus sets the rate relationship between the current mean effective stress p' and the elastic volumetric strain ε_v^e as given

in Equation (4). Using the tangent modulus as a function of the mean stress p', the reference compression modulus K_{ref} and the power parameter m, the volumetric stress–strain relationship given in Equation (6) is obtained.

$$\dot{p}' = -K_t \dot{\varepsilon}_v^e \tag{4}$$

$$K_t = K_{\text{ref}} \left(\frac{p' + p'_t}{p_a} \right)^{1-m} \tag{5}$$

$$\left(\frac{p' + p'_t}{p'_{\text{ref}}} \right)^{m-1} dp' = K_{\text{ref}}\, d\varepsilon_v^e, \tag{6}$$

where p_a and p'_t represent the atmospheric pressure and a compression offset value used to improve the model performance for tension, respectively. Assuming a constant Poisson ratio (υ), one can define a tangent shear modulus G_t (Equation (7)). Non-linear elasticity is defined only in terms of the volumetric components.

$$G_t = \frac{3}{2} K_t \frac{1 - 2\upsilon}{1 + \upsilon} \tag{7}$$

Plastic behaviour is controlled by shear (f_1) and compressive (f_2) yield surfaces that are assumed to be uncoupled (Figure 3a):

$$f_1 = \frac{q'}{R_{1(\theta)}} - \frac{6 \sin \phi}{3 - \sin \phi} (p' + \Delta p') = 0 \tag{8}$$

$$f_2 = (p' + \Delta p')^2 + \frac{2}{9} q'^2 - P_c^2 = 0, \tag{9}$$

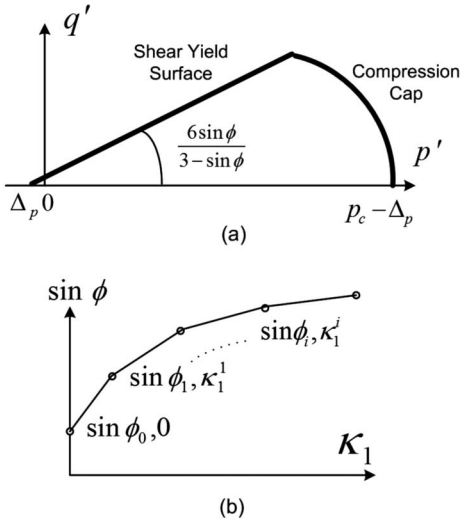

Figure 3. Rockfill constitutive model. (a) Shear and compression yield surfaces in $p' - q'$ space; (b) multi-linear hardening of friction angle w.r.t. internal variable K_1.

where q', ϕ and p_c are the effective deviatoric stress, the friction angle and the preconsolidation pressure, respectively. $\Delta p'$ is a pressure shift introduced to move the shear yield surface, simulating cohesive behaviour. The function $R_1(\theta)$, given in Equation (10), accounts for the difference in the triaxial strength for compression and extension by making use of Lode's angle θ and the factor β_1.

$$R_1(\theta) = \left(\frac{1 - \beta_1 \sin 3\theta}{1 - \beta_1} \right)^{-0.229} \tag{10}$$

$$\beta_1 = \left(\frac{3 + \sin \phi}{3 - \sin \phi} \right)^{\frac{-1}{-0.229}} - 1 \Bigg/ \left(\frac{3 + \sin \phi}{3 - \sin \phi} \right)^{\frac{-1}{-0.229}} + 1 \tag{11}$$

The direction of the inelastic strain rate is determined by the potential surfaces g_1 and g_2, implying an associative behaviour in $p' - q'$ space and a non-associated flow in the deviatoric space.

$$g_1 = q' - \frac{6 \sin \vartheta}{3 - \sin \vartheta} (p' + \Delta p') \tag{12}$$

$$g_2 = (p' + \Delta p')^2 + \frac{2}{9} q'^2 - p_c^2. \tag{13}$$

The dilatancy angle ϑ is a function of the friction angle according to Rowe's stress dilatancy theory, where ϕ_{cv} is a constant value that can be conceived as the friction angle at constant volume.

$$\sin \vartheta = \frac{\sin \phi - \sin \phi_{\text{cv}}}{1 - \sin \phi \sin \phi_{\text{cv}}}. \tag{14}$$

The hardening behaviour for the shear failure surface is modelled through the evolution of the friction angle $\sin \phi = \sin \phi(\kappa_1)$. A multi-linear variation of the friction angle with respect to the internal variable κ_1 is specified (Figure 3b). Both hardening and softening can be simulated with the prescribed multi-linear variation in this formulation (softening terms were not needed/utilised in this study). Changes in κ_1 for the model are tracked using the equivalent plastic deviatoric strain increment $\Delta\gamma^p$ and a diagonal factor matrix $\mathbf{R}$ (Equations (15) and (16)).

$$\Delta\kappa_1 = \sqrt{\left(\frac{2}{3} \right) (\Delta\gamma^p)^T \mathbf{R} (\Delta\gamma^p)} \tag{15}$$

$$\mathrm{R} = \begin{bmatrix} 1 & 0 & 0 & 0 & 0 & 0 \\ 0 & 1 & 0 & 0 & 0 & 0 \\ 0 & 0 & 1 & 0 & 0 & 0 \\ 0 & 0 & 0 & 1/2 & 0 & 0 \\ 0 & 0 & 0 & 0 & 1/2 & 0 \\ 0 & 0 & 0 & 0 & 0 & 1/2 \end{bmatrix}. \quad (16)$$

Because well-documented test results were not available for the filler material of the Cokal dam, test results on the rockfill material from Varadarajan *et al.* (2003) were used to calibrate the material model in this study. The constitutive model was calibrated to triaxial tests that were conducted at three levels of confining stress (i.e. 0.35, 0.7 and 1.1 MPa) using the deviatoric stress-axial strain and the volumetric strain-axial strain results. Hardening of the shear yield surface was prescribed by the multi-linear variation of the sine of the friction angle. The values of the parameters used in the constitutive model are presented in Table 1. A comparison of the model estimates and the triaxial test results is provided in Figure 4.

3.3. *Rockfill-face slab interface*

Experimental data on the behaviour of rockfill-face slab interfaces for CFRD systems are rather limited (Uesugi *et al.* 1990, Zhang and Zhang 2009). Monotonic and cyclic shear tests on the interface were conducted in Uesugi *et al.* (1990); the failure of the interface was decided to be a combination of contact failure and the failure of the granular material beneath with later stages of failure mostly attributed to the first cause. Residual friction coefficients between 0.6 and 0.8 were obtained. A friction-dominated response with volumetric dilation was observed in the tests conducted for the interface between a concrete slab and a gravel cushion layer in Zhang and Zhang (2009). Consistent with the findings of these studies, the interface between the slab and the cushion layer was assumed to be governed by frictional behaviour simulated using a simple Mohr-Coulomb elasto-plastic model (Vermeer and De Borst 1984, TNO DIANA 2008). The Coulomb friction model employs the following yield (f_I) and plastic potential (g_i) surfaces defined in terms of the normal (t_n) and tangential stresses (t_t)

$$f_I = \sqrt{t_t^2} + t_n \tan\phi_I - c_I = 0 \quad (17)$$

$$g_1 = \sqrt{t_t^2} + t_n \tan\vartheta_I \quad (18)$$

where $\tan\phi_I$ and c_1 are the friction coefficient and the cohesion, respectively. $\tan\vartheta_I$ represents the tangent of the angle of dilatancy. The rate of plastic displacement $\Delta\dot{u}^p$ is governed by:

$$\Delta\dot{u}^p = \dot{\lambda}\frac{\partial g}{\partial t}, \quad (19)$$

Table 1. Parameters for the rockfill elasto-plastic model.

Parameter	Value
p'_t	0.2*
$\Delta p'$	0.02*
p_c	1.5*
K_{ref}	13.3*
m	0.22
$\sin\phi(\kappa_1^i)$	0.52 (0.00)**
	0.66 (0.007)
	0.70 (0.014)
	0.74 (0.036)
	0.90 (0.44)
$\sin\phi_{\mathrm{cv}}$	0.755
υ	0.32

Notes: *In MPa; **Refer to Figure 3(b).

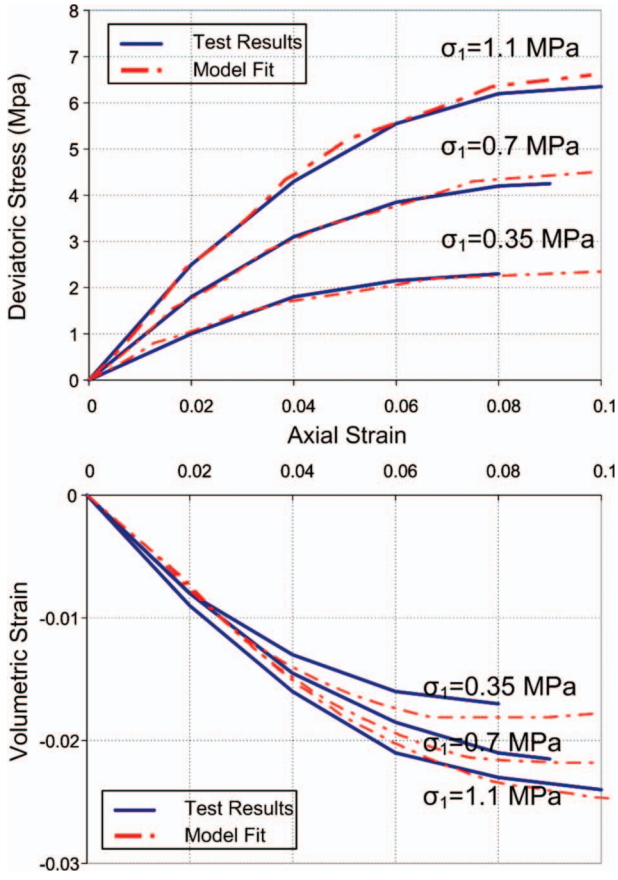

Figure 4. Comparison of triaxial test results (Varadarajan *et al.* 2003) vs. model predictions.

where $\dot{\lambda}$ is a multiplier. The tangent stiffness matrix is non-symmetrical if the friction angle is not equal to the dilatancy angle ($(\phi_I \neq \vartheta_I)$). The interface element was calibrated to the test results given in Zhang and Zhang (2009) for a concrete-gravel layer contact, as shown in Figure 5. Except for the volumetric behaviour in later stages of sliding, which is well beyond the region of interest in this study, the agreement is satisfactory.

3.4. Face slab-plinth interface

A discrete cracking model (TNO DIANA 2008) was used as the constitutive relation for the interface between the face slab and the plinth. Discrete cracking was assumed to take place once the tensile strength, (f_t) of the element was overcome. A brittle failure was assumed with the full reduction of element strength after the exceedance of the tensile strength. The shear stiffness of the interface was also assumed to be reduced to zero once the cracking occurs in this model.

4. Analysis of the Cokal dam for impounding

4.1. Performance of the Cokal dam with preliminary design properties

CFRDs are constructed in 1–2-m thick rockfill layers which are compacted using vibro-cylinders. The majority of the settlement takes place during the construction stage of a CFRD (Kutzner 1997). For most of these systems, the concrete face slab is cast after the construction of the fill is completed. During the impounding, the deformations of a CFRD are small: crest settlements ranging between 0.02–0.05% and 0.1–0.15% of the dam height (H) were provided by Hunter and Fell (2003) and Fell *et al.* (2005) for CFRDs composed of rockfills with very high strength and intermediate strength minerology, respectively. The face slab should be able to conform to these deformations of the dam body without extensive cracking because its performance as a sealing element is a critical aspect of the CFRD behaviour. Deformation of the rockfill can be described as a loading condition on the face slab due to the transfer of stresses between the rockfill and the slab during the settlement of the embankment. Therefore, in order to properly investigate the state of stress on the face slab, (1) the construction sequence, (2) the nonlinear nature of the stress transfer at the interface and (3) the loading stages should be simulated accurately.

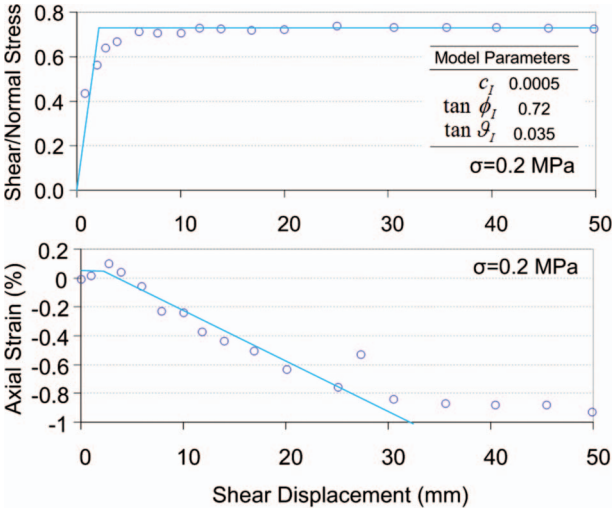

Figure 5. Comparison of shear friction tests (Zhang and Zhang 2009) vs. model predictions.

In this study, the construction of the fill was simulated in 27 stages using 3-m construction increments until the crest height of 83 m was reached. Afterwards, the concrete face slab was created on the top of the rockfill connected to the fill with the interface elements. In the last phase, the impounding of the reservoir was simulated with the reservoir rising in 3 m increments until the maximum water level MWL = 81 m was reached in 27 steps. The sequence of the phased analyses conducted for the Cokal dam is presented in Figure 6.

The horizontal and vertical displacements of the fill (obtained using the rockfill parameters provided in Table 1) for the end of construction (EoC) and the end of impounding (EoI) stages are displayed in Figures 7a,b. A maximum vertical displacement of about 30 cm was observed at the centre of the fill. The displacements caused by the impounding of the reservoir were not significant; the crest of the dam settled around 0.1 m (0.12%H) in line with the estimates from Fell *et al.* (2005). The lateral displacement of the crest was estimated to be around 0.1 m.

The distribution of stresses in the rockfill and the face slab are presented in Figure 8. As given in Figure 8a, impounding changes the vertical stresses on the reservoir side to some extent, but does not change the stresses on the downstream side significantly. The axial stress on the face slab (50-cm thick with a 0.3% reinforcement ratio) was computed at first by assuming a linear elastic face slab behaviour to demonstrate the level of tensile demand on the concrete face slab accurately (Figure 8b). Afterwards, the elastic model was replaced with a total strain fixed crack model (TNO DIANA 2008) in order to determine the extent of cracking within the face slab. (The rockfill material and the interface are modelled using the respective non-linear constitutive models as described in the previous section.) At the EoC stage, the face slab was under compression due to its own weight; the magnitude of this stress linearly increased towards

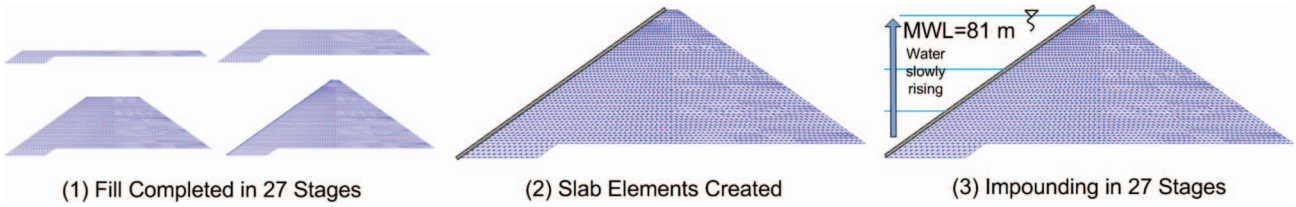

Figure 6. Phased analysis scheme for the construction and impounding stages.

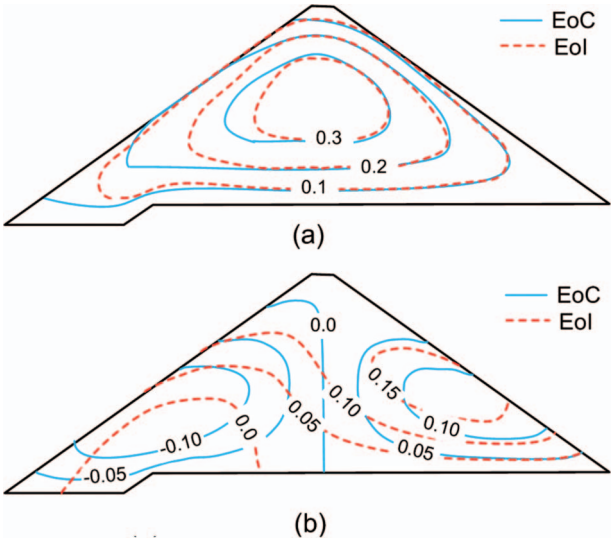

Figure 7. Displacements of the Cokal dam embankment, EoC and EoI stages. (a) Vertical displacement (m); (b) horizontal displacement (m).

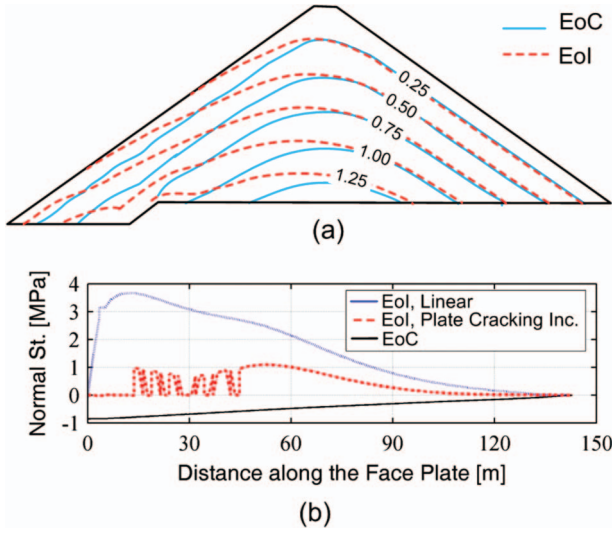

Figure 8. Embankment and face slab stresses for the Cokal dam. (a) Vertical stress (Mpa); (b) stress on the face plate (Mpa).

the plinth to a maximum of 0.9 MPa. At the EoI stage, however, tensile stresses as high as 3.5 MPa were observed for the linear elastic model as a result of the slab being pushed upwards towards the crest due to the reservoir loading and the rockfill deformation. Such a high level of tensile stress necessitates non-linear modelling of the face slab. Using the total strain crack model with embedded reinforcement to model the slab, as much as one-third of the whole slab was observed to be cracked. The jagged appearance of the tensile stress on the slab (Figure 8b) shows the incremental releases of the tensile stress in the slab as is often seen during the cracking of reinforced concrete members.

The cracking of the face plate first starts from the plinth level with the separation of the face slab from the plinth. Cracking starts at this location as the maximum tensile stresses are obtained at the bottom of the slab during the impounding process. At the maximum water level, the opening between the face slab and the plinth was determined to be about 1.0 cm. The separation occurred early in the impounding process, therefore the tensile strength of the cold joint at the plinth, less than that of the face slab concrete, did not affect the analyses results at the maximum water level.

4.2. *Effect of the CFRD rockfill stiffness on the face slab behaviour*

The mechanical properties of the embankment of a CFRD depend on the rockfill mineralogy, particle strength, gradation and construction technique and therefore they are very hard to predict beforehand. In the absence of large triaxial testing of the rockfill material at the site, the designer has to account for the expected variability of the stiffness of the rockfill. Moreover, even if a testing programme is conducted during the construction of a CFRD, the planned gradation of the rockfill cannot be represented exactly in a triaxial test as most of the time relatively larger diameter rock particles ($d_{max} > 15$ cm) are used in the construction of rockfills (Banerjee *et al.* 1979). The mechanical properties of the rockfill also change in time through the contact with water. Selection of an expected range of stiffness for the rockfill is perhaps the most reasonable approach for the design of a

CFRD, such as the range of average modulus of elasticity (25 MPa $< E_{average} <$ 100 MPa) provided in Kutzner (1997).

The calculation of a Young's modulus representing an average stiffness for a rockfill is not a straightforward task as the mechanical properties of the rockfill are strongly dependent on the level of confinement within the embankment. For the Cokal dam, an average Young's modulus was calculated as the mean value of the Young's moduli for each element in the finite element model using the nonlinear elasticity formulation given in Equation (1) for the stress state at the EoI stage. The limited amount of elements in the embankment reaching the yield surface at EoI stage allowed the computation of an equivalent stiffness using this approach. The computed value of $E_{average}$ 50 MPa falls within the range provided above (Kutzner 1997). In order to account for the effect of variability in the stiffness of the rockfill, the lower and upper bounds of the Young's modulus were chosen to be 25 and 100 MPa, respectively, consistent with the aforementioned range. The low modulus of elasticity corresponds to softer rockfills with weak minerology susceptible to cracking and rounding of individual particles while the high modulus of elasticity represents well-prepared rockfills with high strength minerology. In order to achieve this range of stiffness for the rockfill, the weaker and stiffer rockfill conditions were simulated by modifying the model parameters given in Table 1. Only the reference compression modulus and the multilinear hardening relationships were changed from the original parameters shown in Table 2. The simulated deviatoric stress-axial strain behaviours for the 'soft' ($E_{average} = 25$ MPa) and 'stiff' rockfills ($E_{average} = 100$ MPa), which were obtained using the parameters shown in Table 2, are presented in Figure 9 along with the actual test results by Varadarajan *et al.* (2003).

The deformation pattern of the embankment at the centreline is shown in Figure 10 for the assumed range of embankment stiffness. The maximum settlement for the softer fill was 80 cm at the centre of the fill for the EoC stage. The change in the displacements of the embankment after the impoundment was not significant regardless of the stiffness of the rockfill. On the other hand, the lateral displacement at the crest of the dam for the EoI stage was around 0.05 m for the stiffer rockfill condition, increasing up to 0.2 m for the softer case.

The casting of the face slab on the deformed rockfill was simulated for all these cases as described in Figure 6. The change of the axial stress on the face slab during the impounding is presented in Figure 11. At the EoC stage (h = 0), the face slab is subjected to compressive stresses with a maximum value of 1.1 MPa for the soft rockfill ($E_{average} = 25$ MPa). For the stiff rockfill ($E_{average} = 100$ MPa), the maximum compressive stress was around 0.7 MPa. The initial stress on the face slab due to its own weight was therefore larger

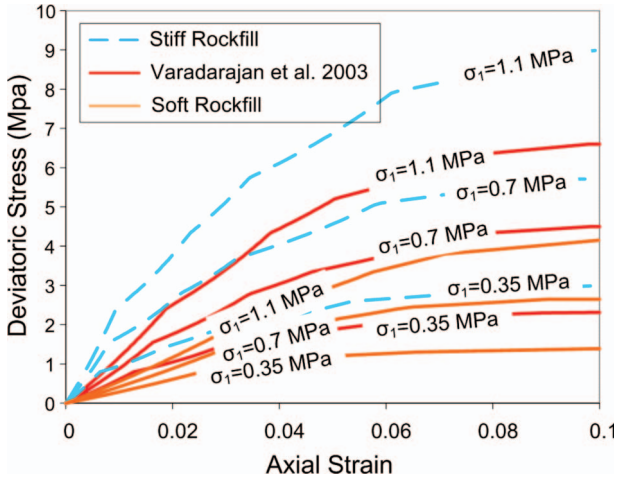

Figure 9. Simulated triaxial tests for a softer and stiffer rockfill compared to Varadarajan *et al.* (2003).

Table 2. Model Parameters for the simulated 'Soft' and 'Stiff' rockfill.

Parameter	Rockfill type		
	Medium	Soft	Stiff
Common parameters	$p'_t = 0.2$ Mpa $\Delta p' = 0.02$ Mpa $p_c = 1.5$ Mpa $m = 0.22$ $\phi_{cv} = 0.755$ $v = 0.32$		
K_{ref} (Mpa)	13.3	6.7	26.6
$\sin\phi(\kappa_1^i)$	0.52 (0.00)	0.52 (0.00)	0.52 (0.00)
	0.66 (0.007)	0.60 (0.007)	0.66 (0.007)
	0.70 (0.014)	0.63 (0.014)	0.72 (0.014)
	0.74 (0.036)	0.65 (0.036)	0.78 (0.036)
	0.90 (0.44)	0.68 (0.44)	0.82 (0.44)

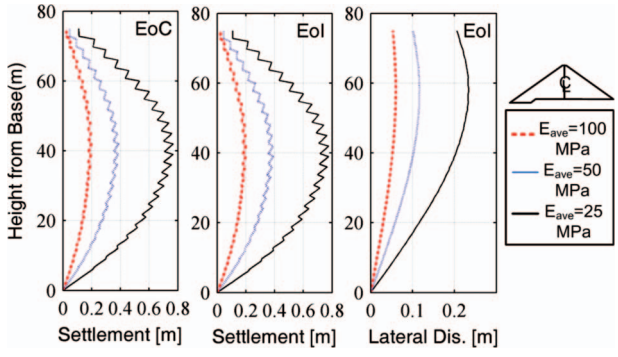

Figure 10. Displacements along the dam centreline for different rockfill stiffness.

for the slab underlain by a softer/weaker rockfill. During the impounding process, the initial compressive stresses decreased gradually and reverted to tensile stresses. At a reservoir level of 42 m, the face slab stresses reached the tensile strength of concrete; cracking was initiated as confirmed by the sudden drop in the stress on the slab (Figure 11). Cracking was observed at the bottom one-third of the face slab at the MWL regardless of the stiffness of the rockfill.

The crack widths on the face slab were estimated using the empirically well-established Gergely–Lutz expression (Gergely and Lutz 1968), which is commonly used in reinforced concrete design (American Concrete Institute (ACI) 2004), relating the maximum crack width w_{max} to three variables: (1) the reinforcement steel strain at the crack (ε_{scr}), (2) the concrete cover over the reinforcement d_c and (3) the area of concrete around each bar A:

$$w_{max} = 2.2\beta_{GL}\varepsilon_{scr}\sqrt[3]{d_c A} \quad (20),$$

where β_{GL} is a factor that accounts for the strain gradient within the member. The crack widths on the face slab at the EoI stage, predicted based on this equation, are shown in Figure 12. As mentioned above, the extent of the cracked region on the face slab was not affected by the stiffness of the embankment. On the other hand, the maximum crack width was reduced significantly when the slab was underlain by a stiffer rockfill. For the softer rockfill ($E_{average} = 25$ MPa) condition, crack widths as large as 2.5 mm were obtained with an average value of about 1.0 mm at the bottom one-third of the slab, while for the stiffer rockfill condition ($E_{average} = 100$ MPa)., maximum and average crack widths were obtained as 0.7 and 0.5 mm, respectively. The average crackwidth (0.6 mm) for the median case ($E_{average} = 50$ MPa) lied in between these estimates.

4.3. *Effect of the interface mechanical properties on the face slab*

The axial stress on the concrete face slab is determined by the load transfer from the rockfill to the slab by the shear friction phenomena. In this section, the sensitivity of this mechanism to the material parameters used to model the friction/contact behaviour, i.e. the friction capacity and the dilation angle, is investigated.

The shear to normal stress ratio at the interface elements between the face slab and the rockfill is presented in Figure 13a for the analyses conducted with different friction capacities at the interface. The upper and lower bounds of the friction capacity at the interface were assumed as 0.8 and 0.6, respectively. At the EoC stage, the friction capacity was reached only at the bottom of the slab for both of these cases; on almost 90% of the slab, the shear stresses did not exceed 40% of the normal stresses. For the EoI stage, the shear stress ratio was further reduced; almost all

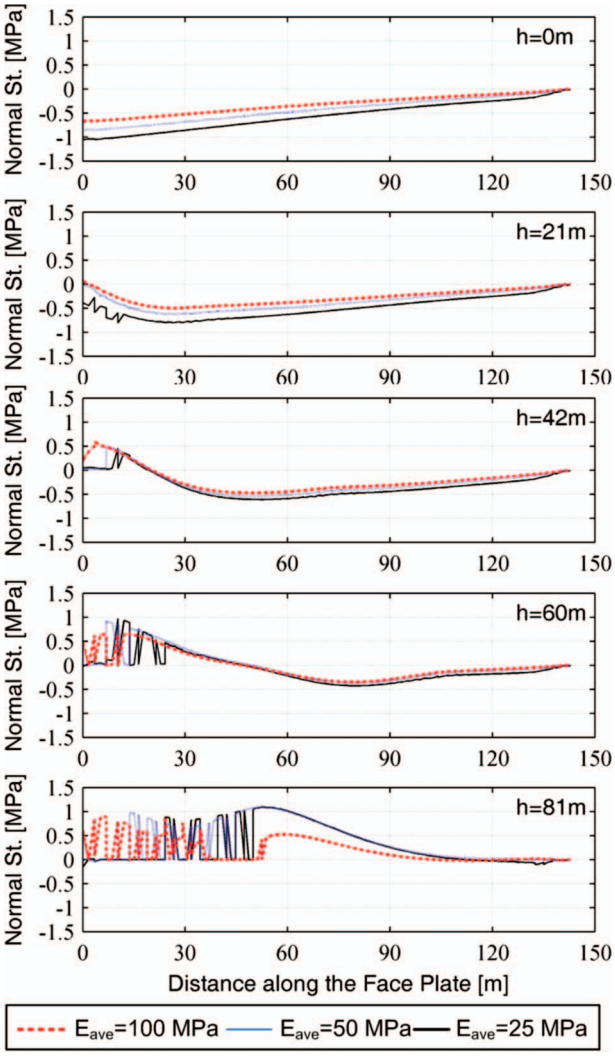

Figure 11. Change in the face slab stress during impounding for different rockfill stiffness.

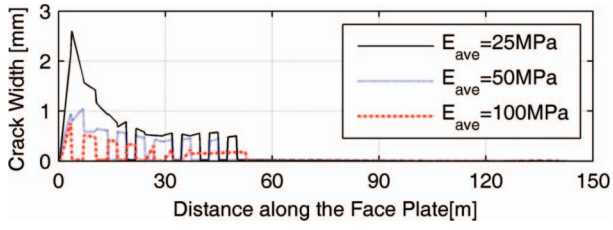

Figure 12. Effect of the rockfill stiffness on maximum crack width on the face slab.

of the slab experienced shear stresses below 10% of the normal stresses. When the friction capacity was assumed lower on the interface, ($\tan\phi_I = 0.6$), the face slab appears to slide on the rockfill in a limited zone near the crest of the dam during impounding. Overall, the capacity of the interface did not seem to affect the stress distribution on the slab significantly as it was only exceeded at a very limited portion of the slab.

In order to investigate the effect of dilation of the interface on the face slab stresses, the shear to normal stress ratio on the face slab was obtained for a range of dilation coefficients for the interface elements (upper bound $\tan\vartheta_I = 0.07$, lower bound $\tan\vartheta_I = 0$) as given in Figure 13b. The friction capacity at the interface was kept at $\tan\theta_I = 0.7$ for these analyses. As the shear stresses on much of the interface remained below the friction capacity, sliding of the slab on the rockfill did not occur; the effect of dilation on the shear stress values was therefore minimal. The distribution of axial stresses on the slab, as provided in Figure 13b, shows that when the dilation angle was reduced at the interface, the cracked region on the slab tended to extend further away from the plinth. However, the effect was not significant enough to justify a clear conclusion on the effect of the dilation characteristics of the interface on the face slab behaviour.

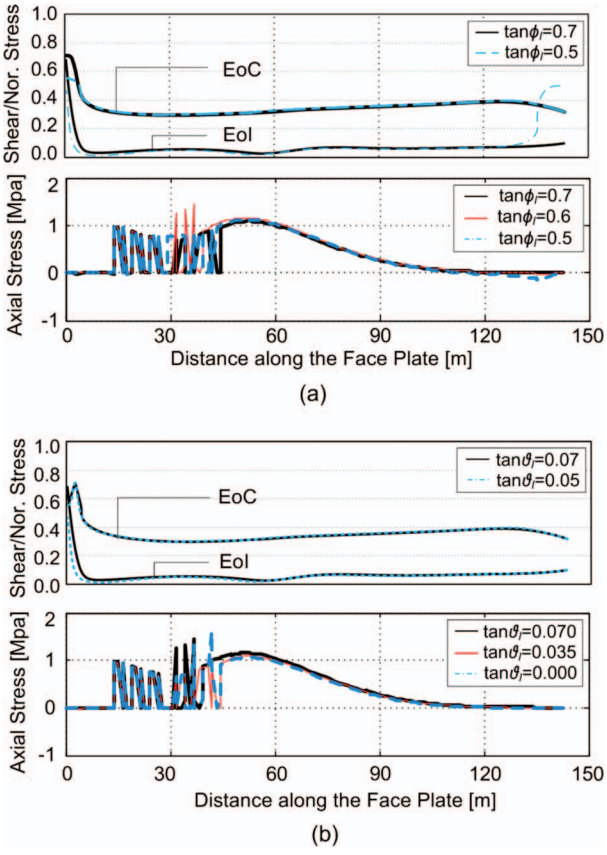

Figure 13. Effect of the interface model parameters on the face slab stress. (a) Variation in the friction angle; (b) variation in the dilation angle.

4.4. *Effect of the design parameters on the face slab performance*

The strength of the concrete slab, the reinforcement ratio, the thickness of the face slab and the clear cover over the reinforcement are the properties of a CFRD that are selected by the designer. The effect of these parameters on the extent of the cracked region and the maximum crack width on the slab is investigated in this section. As shown in Figure 14a, the use of a higher strength concrete for the face slab reduced the spreading of the cracking on the slab. However, the use of C30 concrete ($f'_c = 30$ MPa), compared to C20

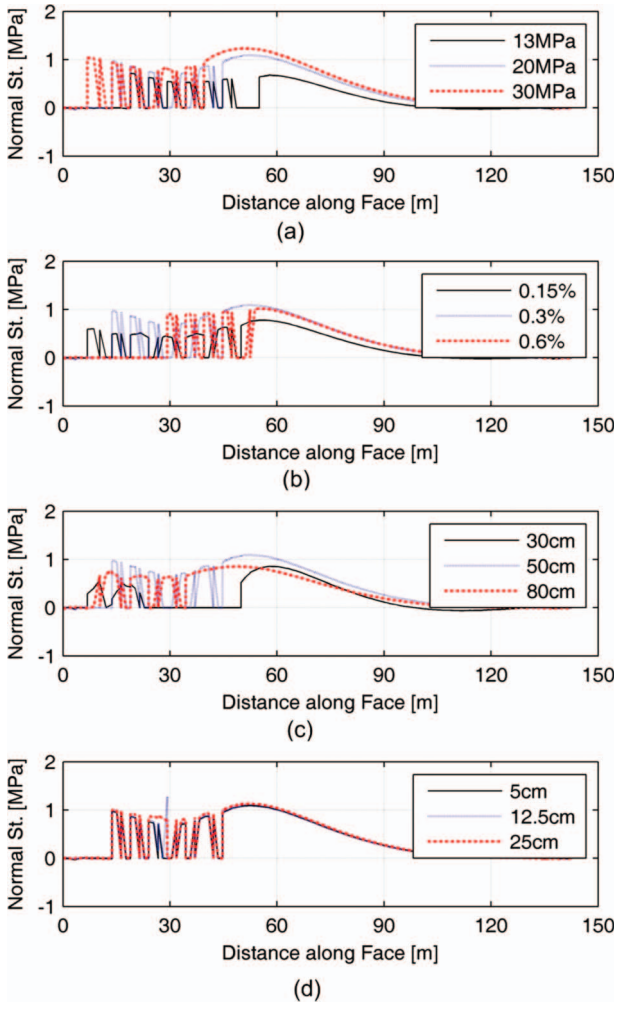

Figure 14. Effect of the design parameters on the face slab stress. (a) The effect of 28 day compressive strength; (b) the effect of reinforcement ratio; (c) the effect of slab thickness; (d) the effect of clear cover on reinforcing steel.

($f'_c = 20$ MPa), decreased the length of the fully cracked region by only 5 m. A correlation between the reinforcement ratio and the extent of the cracked region on the slab was not observed (Figure 14b). The change of the thickness of the slab, on the other hand, changed the extent of the cracked region significantly. Use of an 80-cm thick face slab reduced the extent of the cracked region by 10 m compared to the use of a 50-cm thick slab (Figure 14c). Changing the clear cover over the reinforcement, i.e. placing the reinforcement in the centre or near the surface of the slab, did not affect the length of the cracked region as shown in Figure 14d.

The maximum crack width in the cracked region was directly correlated to the strength of the concrete slab as shown in Figure 15a. Use of a higher strength concrete reduced the spreading of cracks on the face slab as given in Figure 14a, however, at the initiation of cracking, a greater amount of stress was redistributed to the reinforcement causing larger crack widths. The reinforcement ratio of the face slab, as expected, significantly affected the maximum crack width (Figure 15b). Increasing the reinforcement ratio two-folds (from 0.3% to 0.6%) reduced the maximum crack width by almost one half. The maximum crack width did not seem to be changed significantly by the choice of slab thickness or the clear cover over the reinforcement as shown in Figure 15c and d, respectively. However, for the thicker face slabs, the width of the cracks appeared to be larger on a smaller portion of the face slab, compared to the thinner slabs, for which the crack widths decreased but the extent of the cracked portion increased.

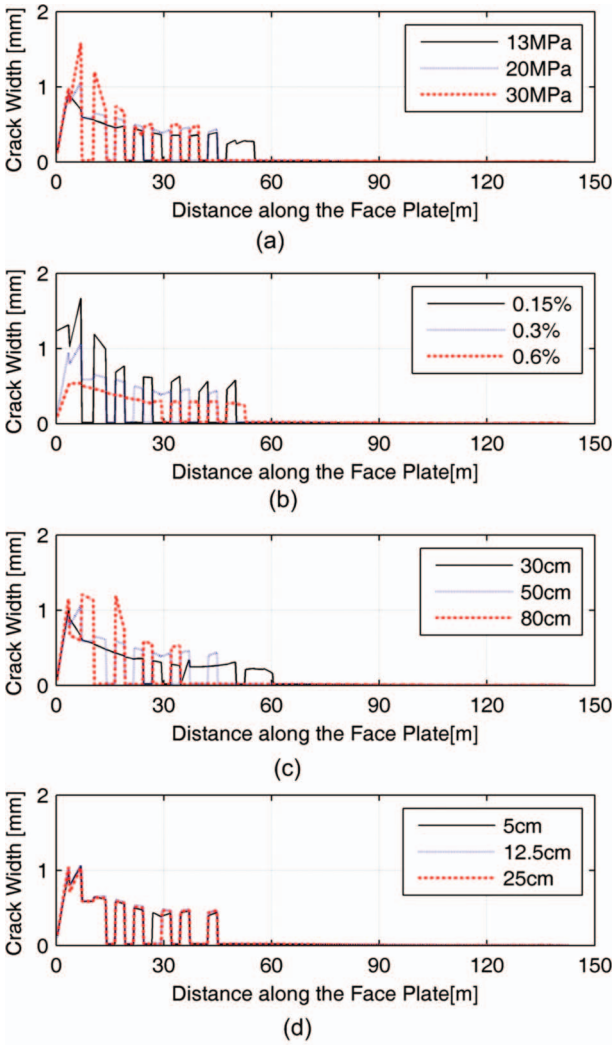

Figure 15. Effect of design parameters on the maximum crack width on the face slab. (a) The effect of 28 day compressive strength; (b) the effect of reinforcement ratio; (c) the effect of slab thickness; (d) the effect of clear cover on reinforcing steel.

4.5. *Comparative study of the relative effects of factors affecting the performance of a face slab*

The relative effects of the various factors that affect the performance of the face slab of a CFRD are compared in this section using an approach called the tornado diagram. Such a diagram is obtained to assess the relative effect of each factor on the behaviour of a system by conducting deterministic sensitivity analyses for the variation in the input properties. For each variable (e.g. reinforcement ratio), two extreme values corresponding to the upper and lower bounds (0.15% and 0.6%) of the selected parameter are used. A variable with a larger effect on the behaviour output has a larger bound of response (swing) than those with smaller effects. For each property, output is obtained twice, using the extreme values for the selected parameter while keeping the other variables at their best (mean) estimates. The extreme values used for the factors in the tornado analysis are presented in Table 3.

Table 3. Bounds on the factors used in tornado analysis.

	Lower bound	Mean property	Upper bound
Rockfill initial modulus (E_{ave}) [Mpa]	25	50	100
Interface friction ($\tan\phi_I$)	0.6	0.7	0.8
Interface dilation ($\tan\vartheta_I$)	0.0	0.035	0.070
Concrete slab thickness (t) [cm]	30	50	80
Concrete 28 day compressive strength f'_c [Mpa]	13	20	30
Reinforcement ratio (%)	0.15	0.3	0.6
Clear cover (cm)	5	12.5	25

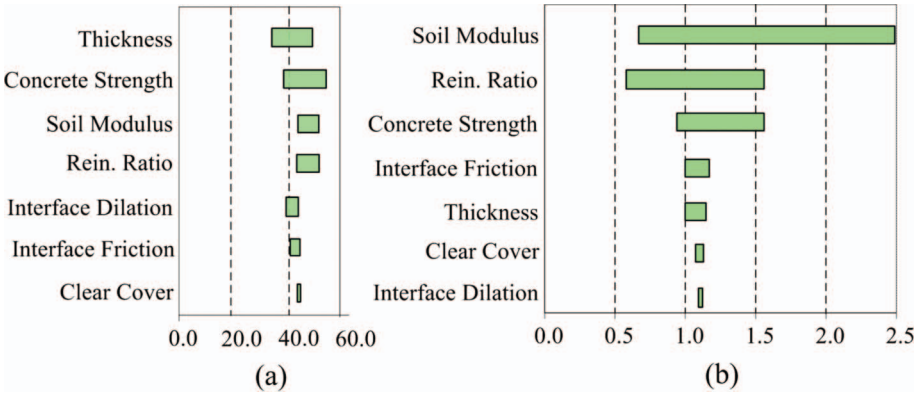

Figure 16. Tornado plot – the relative effects of different factors on the face slab performance. (a) Extent of the cracked region (m); (b) maximum crack width (mm).

The tornado diagram for the extent of the cracked region on the face slab is presented in Figure 16a for the EoI stage. The thickness of the face slab and the concrete strength were obtained as the most important parameters for determining the extent of cracking after the impounding process. The effects of the soil modulus and the reinforcement ratio were smaller relative to the effects of these factors. The properties of the interface and the thickness of the clear cover for the face slab were not significant in determining the extent of cracks. The tornado diagram for the maximum crack width on the face slab is presented in Figure 16b. The factors greatly affecting the maximum crack width were the soil modulus and the reinforcement ratio of the face slab. For a softer rockfill, one can expect significantly larger crack widths on the slab. Increasing the reinforcement ratio appears as the best design remedy for addressing this behaviour. The strength of the face slab concrete also affected the maximum crackwidth to some extent, however, other factors (interface properties, clear cover thickness, the thickness of the slab) did not affect the maximum crackwidth significantly.

5. Results and conclusions

In this study, the performance of the face slab of a CFRD was investigated considering the variability in the rockfill properties and the design choices for the concrete face slab. The following provides a short summary of the conclusions of this study.

- At the EoI stage, an average crack width of 0.6 mm was obtained for the Cokal dam, built using rockfill with an average modulus of E_{average} 50 MPa and a 50-cm thick concrete face slab with a 0.3% reinforcement ratio. Cracking at the bottom spread to almost one-third of the face slab. The average crackwidth is higher than the suggested value (0.1 mm) for corrosion prevention in ACI-318-05 (ACI 2004).
- Crack widths obtained on the face slab of the Cokal dam increased considerably when the rockfill was assumed to be of lower stiffness in the simulations. As expected, both the maximum and average crack widths were reduced with the increase in the rockfill stiffness in the simulations.
- Increasing the reinforcement ratio appears to be the most effective way of reducing the crack width in the cracked region of the face slab for a CFRD. However, increasing the reinforcement ratio did not significantly change the extent of the cracked region on the face slab.
- Increasing the thickness of the face slab limited the spreading of the cracking towards the dam crest to some extent. However, the use of a thicker face slab (50 or 80 cm) did not significantly change the predicted maximum crack width.
- The friction capacity of the interface layer between the rockfill and the face slab, as well as its dilation characteristics, did not seem to significantly affect the stresses on the face slab. During the impounding process, the maximum crack width and the extent of the cracked region were not affected significantly from the variability in these properties.
- In conclusion, an increase in the reinforcement ratio of the face slab of a CFRD was determined to be the optimal remedy for the controlling of the cracking of its face slab. Especially for the CFRDs whose embankments are susceptible to have a low stiffness due to the minerology or the preparation of the rockfill, an increase in the reinforcement ratio over the conventional practice may be very beneficial for the long-term performance of the system.

Acknowledgements

This study has been conducted with the funding provided by The Scientific and Technological Research Council of Turkey (TUBITAK) under the grant MAG108M491.

References

American Concrete Institute (ACI) 318: 2004. *Building code requirements for structural concrete and commentary 2005*. Farmington Hills, MI: ACI.

Banerjee, N.G., Seed, H.B., and Chan, C.K., 1979. *Cyclic behavior of dense coarse grained sands in relation to seismic stability of dams*. Rep No 79/13. Berkeley, CA: EERC.

Bayraktar, A. and Kartal, M.E., 2010. Linear and nonlinear response of concrete slab on CFR dam during earthquake. *Soil Dynamics and Earthquake Engineering*, 30, 990–1003.

Cooke, B., 1986. Progress in rockfill dams. *In*: Executive Committee of the Geotechnical Engineering Division of the American Society of Civil Engineers, John T. Christian, Chairman, *Geotechnical special publication no.1, terzaghi lectures*. New York, NY: ASCE, 363–394.

Feenstra, P.H., *et al*., 1998. A 3D constitutive model for concrete based on a co-rotational concept. In: B.B.R. de Borst *et al*., eds. *EURO-C 1998, computer modeling of concrete structures*. Rotterdam: Balkema, 13–22.

Fell, R., *et al*., 2005. *Geotechnical engineering of dams*. Rotterdam, the Netherlands: Balkema.

Gergely, P. and Lutz, L.A., 1968. Maximum crack width in reinforced concrete flexural members. *In*: *Causes, mechanism and control of cracking in concrete, SP20*. Detroit, MI: American Concrete Institute, 87–117.

Groen, A.E., 1995. *Elastoplastic modelling of sand using a conventional model*. Tech. Rep. 03.21.0.31.34/35. Delft, the Netherlands: Delft University of Technology.

Hunter, G. and Fell, R., 2003. Rockfill modulus and settlement of concrete face rockfill dams. *Journal of Geotechnical and Geoenvironmental Engineering*, 129 (10), 909–917.

ICOLD, 2004. *Concrete face rockfill dams concepts for design and construction*. Paris, France: ICOLD Commitee on Materials for Fill Dams.

Johannesson, P. and Tohlang, S.L., 2007. Lessons learned from Mohale. *International Water Power and Dam Construction* [online]. Available from: http://www.waterpowermagazine.com [Accessed 29 March 2011].

Kutzner, C., 1997. Earth and rockfill dams. Rotterdam, the Netherlands: Balkema.

Qian, C., 2005. Recent development of concrete faced rockfill dams in China. *In*: *Proceedings of the symposium on 20 years (1985–2005) of Chinese CFRDs construction*. Yichang, China, 8–14.

TNO DIANA, 2008. *User's manual, R. 9.3*. Delft, the Netherlands: TNO DIANA.

Uddin, N., 1999. A dynamic analysis procedure for concrete-faced rockfill dams subjected to strong seismic excitation. *Computers and Structures*, 72, 409–421.

Uesugi, M., Kishida, H., and Uchikawa, Y., 1990. Friction between dry sand and concrete under monotonic and repeated loading. *Soils and Foundations*, 30 (1), 115–128.

Varadarajan, A., *et al*., 2003. Testing and modeling two rockfill materials. *Journal of Geotechnical and Geoenvironmental Engineering*, 129 (3), 206–218.

Vermeer, P.A. and De Borst, R., 1984. Non-associated plasticity for soils, concrete and rock. *Heron*, 29 (3), 3–64.

Wieland, (2010). CFRDs in highly seismic regions. *International Water Power and Dam Construction* [online]. Available from: http://www.waterpowermagazine.com [Accessed 29 March 2011].

Zhang, G. and Zhang, J.M., 2009. Numerical modelling of soil-structure interface of a concrete face rockfill dam. *Computers and Geotechnics*, 36 (5), 762–772.